

## APPLICATION NOTE

# Imaging antiferromagnetic spin cycloids in bismuth ferrite (BiFeO<sub>3</sub>) with the Qnami ProteusQ

Potential applications: antiferromagnets, multiferroics, weak ferromagnets

Related products: Qnami ProteusQ™ , Quantilever™MX

Release date: 19 June 2020

## 1 Motivation

Antiferromagnets are magnetically ordered materials, where the directions of the atomic magnetic moments alternate, resulting in net macroscopic magnetization which is nominally zero. Beyond their fundamental interest, antiferromagnets present attractive features for future spintronic applications [1]. They are largely insensitive to external parasitic magnetic fields, and exhibit domains (potentially usable as bits) which have almost no cross-talk and can be switched at high speeds (switching frequencies are in the THz regime). Furthermore, in multiferroics, where in some cases antiferromagnetism coexists with ferroelectricity, it is possible to control the magnetic state electrically - a very appealing feature for device applications.

It is largely overlooked that these seemingly exotic materials are in fact widespread - a 90% majority of known magnets present such antiferromagnetic order. Well-studied examples include many metal-oxides, manganese-based alloys and rock salts as well as halides. Yet, the real-space observation of antiferromagnetic order remains a challenging task, in particular at the nanoscale. On the one hand, high resolution imaging techniques such as x-ray magnetic circular dichroism (XMCD) and x-ray magnetic linear dichroism

(XMLD) making use of large-scale synchrotron facilities, or the conventional table-top magnetic force microscopy techniques fall short in sensitivity. On the other hand spin-polarized scanning tunneling microscopy (SP-STM) and magnetic exchange force microscopy (MExFM) are operating in complex cryogenic and/or ultra-high vacuum conditions.

However, it was recently realized that high-sensitivity magnetic imaging of the stray fields (also known as demagnetizing fields) outside the material offers a powerful avenue to address nanoscale spin textures in antiferromagnets. While this may appear surprising at first, it has been long known that symmetry breaking in antiferromagnets, as encountered on surfaces, domain-walls or the like, give rise to small uncompensated magnetic moments in the material, which can then be addressed by stray magnetic field imaging. Specifically, Gross et al. revealed for the first time the complex magnetic order at the surface of BiFeO<sub>3</sub> using scanning nitrogen-vacancy magnetometry (SNVM) techniques [2]. This result represents an important breakthrough in the investigation of antiferromagnets and multiferroics for applications in low power spintronics devices, which triggered active research [3, 4].

In this Application Note, we show how Qnami ProteusQ™ can be used to image antiferromagnetic spin textures with state-of-the-art accuracy. We present two modes of operation allowing to rapidly converge towards quantitative understanding of the magnetic textures at the surface of an antiferromagnet. We use BiFeO<sub>3</sub> as a prototype example, where we reveal spin cycloidal antiferromagnetic order with a performance that compares favorably with the recent literature.

## 2 Sample

We conduct our case-study on a strained BiFeO<sub>3</sub> film<sup>1</sup> with a thickness of  $t_{\text{BiFeO}_3} = 54$  nm. The sample has an overall footprint of  $5 \times 5$  mm<sup>2</sup> and presents  $\mu\text{m}^2$  large atomically flat areas (shown in later AFM results). The BiFeO<sub>3</sub> sample is mounted in the Qnami ProteusQ™ using our specifically developed non-magnetic sample holder.

The spin cycloid, corresponding to the rotation of a weak ferromagnetic moment  $m_{\text{eff}}$ , is one of the distinguishing features of the magnetic order in BiFeO<sub>3</sub>. This rotation results from the canted antiferromagnetic arrangement of individual Fe<sub>3</sub><sup>+</sup> electron spins in adjacent planes and propagates with a direction  $k$  and a wavelength  $\lambda$  typically smaller than 100 nm (see simplified model in Fig.1). Eventually, the whole sample can be considered as stack of planes with such cycloidal magnetic moments.

## 3 Experimental procedure

The operating principle of the Qnami ProteusQ™ scanning NV magnetometer is described in Fig.2. A diamond tip containing a single NV center is mounted onto a tuning-fork and kept fixed while the sample is scanned with sub-nanometer precision. A high numerical aperture objective (NA = 0.7) is used to collect NV fluorescence. A near-field microwave antenna is brought in close proximity to probe the NV-spin resonance and perform optically detected magnetic resonance (ODMR) measurement. The axial bias magnet integrated onto the objective lens allows to determine the polarity of the measured magnetic field.

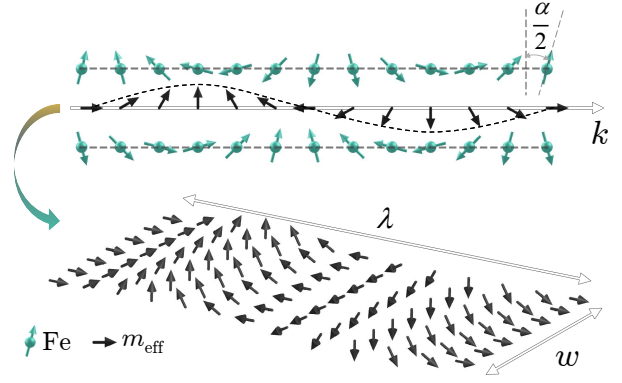


**Fig. 1: Simplified model of the spin-cycloid in BiFeO<sub>3</sub>.** The antiferromagnetically ordered Fe spins (green) exhibit a slight canting (by the canting-angle  $\alpha$ ), which leads to a net effective magnetic moment  $m_{\text{eff}}$  (black arrows). This net moment exhibits a rotation in space with wavelength  $\lambda$  and along a wave-vector  $k$ . It is this resulting spin-cycloid which in the focus of this application note and which we address by virtue of stray-field imaging using scanning NV magnetometry.

### 3.1 Quantilever™MX

We performed the study using a Quantilever™MX probe containing a single NV center implanted with 6 keV of energy (nominal NV depth<sup>2</sup>: 10 nm). The Quantilever is mounted onto the ProteusQ probe holder and inserted into the apparatus using Qnami's rapid tip-exchange mechanism. After adjusting the focus of the objective, the Quantilever can be readily seen in the wide-field (WF) image (Fig.3a).

### 3.2 NV fluorescence imaging

Scanning NV Magnetometry relies on optical read out of the fluorescence from the single NV center embedded at the Quantilever tip apex. To ensure the highest sensitivity, it is important to optimize the collection efficiency of the NV fluorescence. This is achieved through two automatized steps in the LabQ software. First a confocal fluorescence image is acquired. The result is shown in Fig.3b, where the diamond pillar position appears as a bright spot. A built-in function further aligns the collection optics to this spot and tracks the optimum along the measurements.

<sup>2</sup>Quantilevers MX with different implantation energies are available at Qnami. For a given Quantilever MX series, the *nominal* NV depth is calculated from the parameters of implantation using SRIM (<http://www.srim.org>) and represents a lower-bound estimation of the actual NV depth.

<sup>1</sup>Sample courtesy of Unité Mixte de Physique CNRS/Thales, Paris, France.

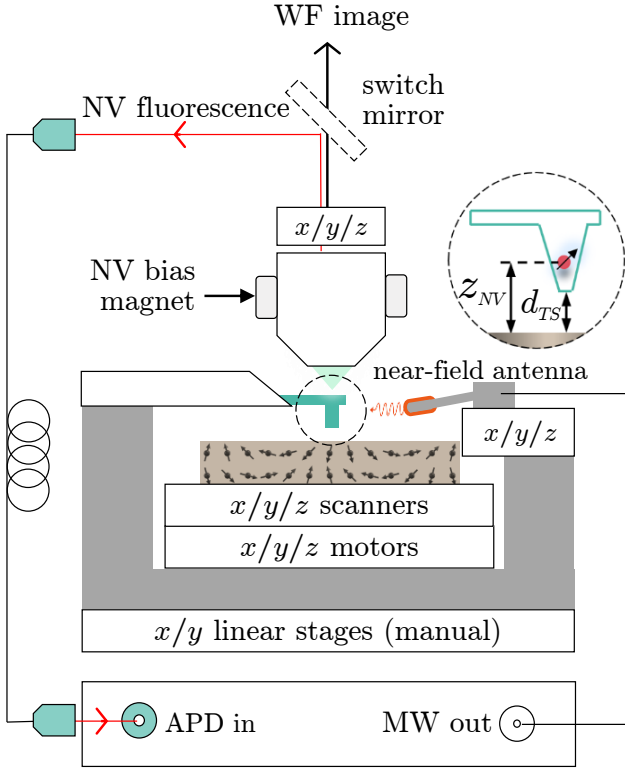


**Fig. 2: Scanning NV magnetometer.** At the core of the measurement apparatus is the diamond probe containing a single NV center and mounted on a tuning-fork force sensor (Quantilever, in green). The NV center is excited by a green laser (not shown) and its fluorescence collected by a NA = 0.7 top objective and sent to an avalanche photodiode (APD). The sample is positioned onto the piezo scanners and step motors allowing for fine and coarse adjustment in all three directions. A video microscope channel equipped with LED illuminator and CMOS camera allows wide-field (WF) imaging of the quantilever and sample surface. During raster scan, ODRM spectra are obtained by sweeping the MW frequency of the near-field antenna.

### 3.3 Optically detected magnetic resonance (ODMR) spectroscopy

A central concept in SNVM is the ability to determine the electronic spin resonance (ESR) of the NV center at each pixel of a raster scan. This is achieved through optically detected magnetic resonance (ODMR). To perform ODMR spectroscopy, the microwave (MW) near-field antenna is brought in proximity ( $< 50 \mu\text{m}$ ) to the Quantilever (Fig. 2). An integrated side-view CCD camera and the miniaturized  $x/y/z$  manual stage are used for this alignment in a streamlined and reliable way.

A typical ODMR spectrum is shown in Fig. 3c, where the fluorescence count-rate of the NV center

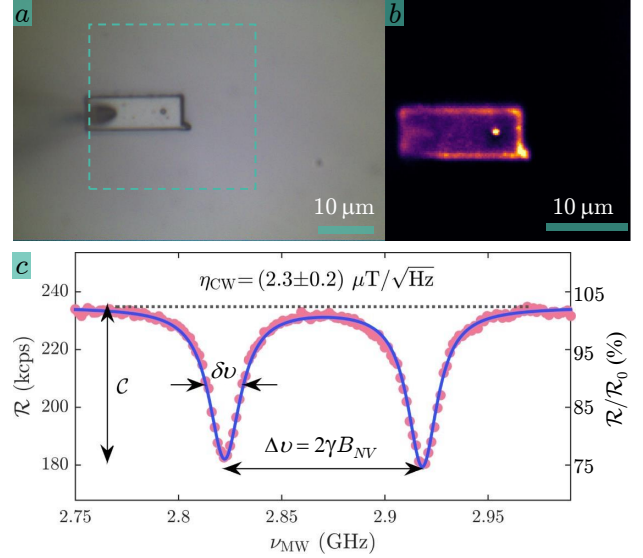


**Fig. 3: Alignment steps and ODMR spectrum.**

(a) After inserting the Quantilever into the system, the optical focus is adjusted to visualize the diamond device on the integrated CMOS camera. (b) An automatic optical confocal scan yields a 2D fluorescence map of the device. The optics is further adjusted automatically in order to maximize NV photon collection and measurement sensitivity. (c) ODMR spectrum. The two resonances reveal a Zeeman splitting corresponding to  $B_0 = 1.8 \text{ mT}$  generated by the bias magnet. The high photon count-rate ( $R_0 > 230 \text{ kcps}$ ), large ESR contrast ( $C > 25\%$ ) and narrow linewidth ( $\delta\nu \sim 9 \text{ MHz}$ ) are typical values for the Quantilever<sup>TM</sup>MX probe, resulting an excellent detection sensitivity of  $\eta = 2 \mu\text{T}/\sqrt{\text{Hz}}$ .

is recorded as a function of the MW frequency. We observe two resonances separated by  $\Delta\nu = 100 \text{ MHz}$ . Using

$$\Delta\nu = \nu_1 - \nu_2 = 2\gamma_{\text{NV}}B_{\text{NV}} \quad (1)$$

with  $\gamma_{\text{NV}} = 28 \text{ GHz/T}$ , we determine the magnetic field component  $B_{\text{NV}}$  along the NV axis in a quantitative, self-calibrated way. We find here  $B_0 = 1.8 \text{ mT}$ , which corresponds to the bias magnetic field generated by the bias magnet field at the location of the NV center (see Fig. 2). Finally, we calculate the magnetic field sensitivity  $\eta$ , [5] corresponding to our experimental conditions using

$$\eta = \frac{4}{3\sqrt{3}} \frac{h}{g\mu_B} \frac{\delta\nu}{C\sqrt{R_0}} \quad (2)$$

where  $h$ ,  $g$  and  $\mu_B$  are respectively the Planck constant, the Landé factor and the Bohr magneton,  $\delta\nu$  is the ESR linewidth,  $R_0$  the count-rate away from resonance and  $C$  the contrast in the ODMR

curve. Using the values from Fig. 3c, we find a magnetic-field sensitivity  $\eta = 2.3 \pm 0.2 \mu\text{T}/\sqrt{\text{Hz}}$

### 3.4 AFM parameter settings in SNVM

The Qnami ProteusQ<sup>TM</sup> operates with a tuning-fork (TF). We use here the frequency modulation mode (FM-AFM). The frequency shift  $\Delta f$  of the TF resonance frequency serves as feedback signal (error signal) for stabilizing the tip-to-sample distance  $d_{\text{TS}}$ .  $d_{\text{TS}}$  is decreased (increased) by increasing (decreasing)  $\Delta f$ . After a preliminary AFM scan over a  $20 \times 20 \mu\text{m}^2$  area, we identify an atomically flat area and set the frequency shift to  $\Delta f = 15 \text{ Hz}$ , ensuring the smallest flying distance (estimated  $d_{\text{TS}} < 5 \text{ nm}$ ) thereby ensuring maximum sensitivity and spatial resolution.

## 4 Measurements

We first present the iso-B mode, which allows for rapid visualization of the magnetic textures, and then introduce the full-B mode, which allows for a full quantitative analysis of the stray field.

### 4.1 Rapid investigation through iso-B imaging

Fig. 4 shows a  $700 \times 700 \text{ nm}^2$  wide Iso-B image, obtained by recording the NV fluorescence as the Quantilever is scanned over the sample, with a fixed MW frequency  $\nu_{\text{iso}} = 2813.5 \text{ MHz}$  applied. At each pixel, the NV center experiences a magnetic field  $B_{\text{NV}}(x, y) = B_0 + B_{\text{sample}}(x, y)$ . Whenever  $B_{\text{NV}}(x, y) = \nu_{\text{iso}}/2\gamma_{\text{NV}}$  (the resonance condition), the MW induces a population transfer in the NV spin state, which reduces the fluorescence count-rate by  $C = 25\%$ . In the final map, regions of reduced NV fluorescence are then identified as regions where  $B_{\text{sample}}(x, y) = \nu_{\text{iso}}/2\gamma_{\text{NV}} - B_0 = 115 \mu\text{T}$ .

The measurement readily reveals a periodic stray field pattern corresponding to the expected spin cycloidal textures in the BiFeO<sub>3</sub>. Remarkably, the data also reveal an additional, “zigzag” shaped modulation on the periodic stray field. Such modulations were already observed in Ref [2], and assigned to changing cycloid wave-vector directions due to the presence of ferroelectric domains in the material.

In conclusion, the iso-B imaging mode is an excellent tool for rapid sample exploration, in par-

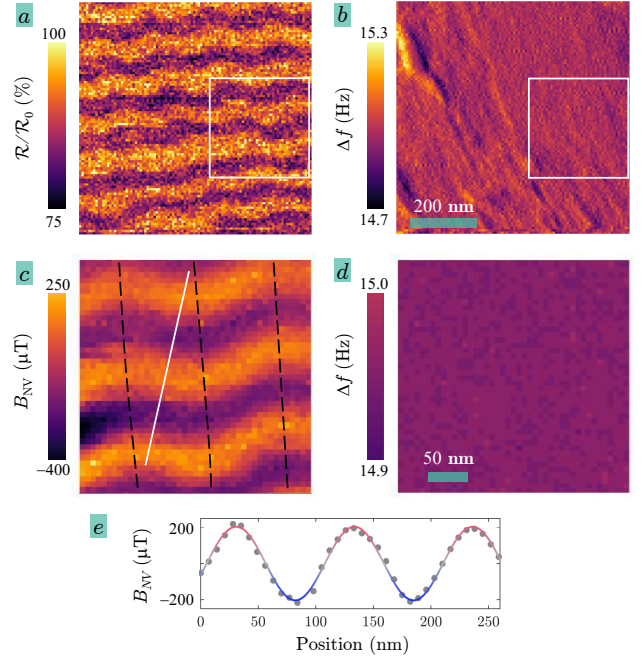


**Fig. 4: SNVM measurements on BiFeO<sub>3</sub>.** (a) iso-B map. The dark features correspond to magnetic field contour of  $B_{\text{sample}} = 115 \mu\text{T}$  (integration time 10 ms/pixel;  $200 \times 200 \text{ pixel}^2$ ; total acquisition time  $\sim 13 \text{ min}$ ). (b) simultaneously recorded frequency shift error signal images. An atomically flat area (surface roughness of 0.45 nm r.m.s) is identified (square region) for further full-B mode imaging. (c) full-B image ( $45 \times 45 \text{ pixel}^2$ ) shows a full quantitative map of  $B_{\text{Sample}}(x, y, z_{\text{NV}})$  (pixel dwell time 4.5 sec/pixel corresponding to a total acquisition time of 2.5 hours). The dashed lines are guides to the eye and demarcate regions with different cycloid wave vector  $k$  (associated with the presence of different ferroelectric domains [2]). (d) Corresponding error signal image. (e) Line cut along the cycloid propagating direction (white line in (c)). A simple sinusoidal fit yields a propagation wavelength  $\lambda = 102.7 \pm 0.8 \text{ nm}$ .

ticular in materials where only weak stray field signals exist, such as in antiferromagnets. By restricting the measurement to a single value of the stray field, one can perform large range scans in minimum time. In our example, Fig. 4 was recorded in 13 minutes including both forward and backward scans (pixel dwell time of 10 ms). This acquisition time compares well with AFM/MFM standards. It should be noted however, that the iso-B mode provides contrast over a limited dynamical range associated with the linewidth of the electron spin resonance.

## Advantages of Qnami ProteusQ™ for imaging antiferromagnets

Scanning NV Magnetometry provides unique insights into antiferromagnetic materials such as the BiFeO<sub>3</sub> example studied in this application note. Success in imaging the magnetic textures at the surface of antiferromagnets such is guaranteed by the following unique properties of the Qnami ProteusQ™ :

- **High sensitivity: detect the smaller signals.**

The sensitivity of Qnami ProteusQ™ is on the order of  $1 \mu\text{T}/\sqrt{\text{Hz}}$ , as demonstrated in Fig.3c.

- **High spatial resolution: observe the smallest lateral features.**

Qnami ProteusQ™ offers spatial resolution  $< 50 \text{ nm}$ .

- **Ultra-low thermal drift: guaranteed stability over long-term measurement.**

Stable mechanical design by HORIBA coupled with the full close-loop operation offers the lowest drift rates ( $< 2 \text{ nm/h}$  over 24 h).

- **All-in-one ODMR control: MicrowaveQ controller included.**

Single photon counting and digital microwave controller designed for ODMR spectroscopy of NV centres.

- **Intuitive software interface: LabQ software included.**

Alignment routines, auto-track fluorescence mode, user-friendly measurement mode.

### 4.2 Quantitative analysis through full-B mode image

A full-B image recorded over a region of  $280 \times 280 \text{ nm}^2$  is shown in Fig.4c. In this mode, a complete ODMR spectrum is recorded at each pixel and the exact value  $B_{NV}$  of the magnetic field projection along the NV axis is extracted from the splitting  $\delta\nu$ . In order to obtain such high quality, quantitative data, the integration time was increased to 4.5 sec/pixel for a total measurement time of 2 hours. We point out the excellent stability and close-loop operation of Qnami ProteusQ™ resulting in drift rate  $< 2 \text{ nm/h}$  over a period of 24 h.

In such data one can here recognize the same periodic patterns as already observed with the iso-B mode. However, the quantitative nature of this magnetic stray field image allows for further physical insight and, in conjunction with suitable models, the extraction of material parameters from the sample. In the specific case of the BiFeO<sub>3</sub> cycloid, for example, a model fit to such quantitative data allowed for the extraction of the effective magnetic moment  $m_{\text{eff}}$  (c.f. Fig. 1) of the spin cycloid, which was found to be on the order of 0.07 Bohr magnetons per BiFeO<sub>3</sub> unit cell [2]. In addition, careful analysis of such quantitative data enabled the discovery of a previously unknown magnetic interaction term in BiFeO<sub>3</sub> – a so-called Dzyaloshinskii–Moriya exchange interaction - rele-

vant to understand its magnetic order [2]. These findings and the data quality that can be obtained in such full-B NV magnetic imaging demonstrate the power of the technique and the added value it brings to research in the field of nanomagnetism.

## 5 Summary

In this application note, we have demonstrated the qualitative and quantitative imaging of spin cycloids in the multiferroic material BiFeO<sub>3</sub>, using the table-top Qnami ProteusQ scanning NV magnetometer. These results showcase the sensitivity and spatial resolution which can readily be achieved with the functionalities of Qnami’s solution. Our unique, state-of-the-art platform for real-space, nanoscale magnetic imaging offers access to non-trivial spin textures which would be largely inaccessible otherwise. In the case of BiFeO<sub>3</sub>, this already had profound scientific impact in that such direct, real-space imaging, together with theoretical modelling of the underlying spin-structure, revealed the presence of previously unobserved Dzyaloshinskii–Moriya interactions in BiFeO<sub>3</sub>. In the same vein, the non-invasive and quantitative imaging capabilities of the Qnami ProteusQ™ are poised to yield fundamental insights and practical information for a variety of other materials exhibiting antiferromagnetic order. Indeed, uncompensated magnetic moments in antiferromagnetic systems appear to form the norm, rather

than the exception and allow for direct, real space imaging of antiferromagnetic order by nanoscale magnetometry. We therefore anticipate the Qnami ProteusQ™ to enable range of new insights into the physics of antiferromagnets, their domains and spin textures. This will not only advance our fundamental understanding of antiferromagnets but ultimately also inform new device architectures in the emerging field of antiferromagnetic spintronics.

## Acknowledgement

We are grateful to Dr. K. Bouzehouane, S. Fusil, J. Fischer, Dr. V. Garcia from the Unité Mixte de Physique CNRS and Thales (Paris, France) and A. Haykal from the Laboratoire Charles Coulomb at the University of Montpellier for providing state of the art BiFeO<sub>3</sub> samples as well as for fruitful discussions.

## References

- <sup>1</sup>V. Baltz, A. Manchon, M. Tsoi, T. Moriyama, T. Ono, and Y. Tserkovnyak, “Antiferromagnetic spintronics”, *Reviews of Modern Physics* **90** (2018).
- <sup>2</sup>I. Gross, W. Akhtar, V. Garcia, L. J. Martinez, S. Chouaieb, K. Garcia, C. Carrétéro, A. Barthélémy, P. Appel, P. Maletinsky, J.-V. Kim, J. Y. Chauleau, N. Jaouen, M. Viret, M. Bibes, S. Fusil, and V. Jacques, “Real-space imaging of non-collinear antiferromagnetic order with a single-spin magnetometer”, *Nature* **549**, 252–256 (2017).
- <sup>3</sup>J.-Y. Chauleau, T. Chirac, S. Fusil, V. Garcia, W. Akhtar, J. Tranchida, P. Thibaudeau, I. Gross, C. Blouzon, A. Finco, M. Bibes, B. Dkhil, D. D. Khalyavin, P. Manuel, V. Jacques, N. Jaouen, and M. Viret, “Electric and antiferromagnetic chiral textures at multiferroic domain walls”, *Nature Materials* **19**, 386–390 (2019).
- <sup>4</sup>A. Haykal, J. Fischer, W. Akhtar, J.-Y. Chauleau, D. Sando, A. Finco, F. Godel, Y. A. Birkhölzer, C. Carrétéro, N. Jaouen, M. Bibes, M. Viret, S. Fusil, V. Jacques, and V. Garcia, “Antiferromagnetic textures in BiFeO<sub>3</sub> controlled by strain and electric field”, *Nature Communications* **11** (2020).
- <sup>5</sup>L. Rondin, J.-P. Tetienne, T. Hingant, J.-F. Roch, P. Maletinsky, and V. Jacques, “Magnetometry with nitrogen-vacancy defects in diamond”, *Reports on Progress in Physics* **77**, 056503 (2014).



Address Qnami AG  
Hofackerstrasse 40B  
4132 Muttenz  
Switzerland

Website [www.qnami.ch](http://www.qnami.ch)

## DISCLAIMER

The content of this document is copyrighted by Qnami AG. Qnami AG makes no warranties with respect to the accuracy or completeness of the content in this document and reserves the right to make changes to the specification at any time without notice. All trademarks are the property of the company Qnami AG.

Qnami AG © 2017 – 2020